RESEARCH ARTICLE

Ionic Liquid-Assisted Synthesis, Characterization and Photocatalytic Properties of SnO Microflowers with Nanosheet Subunits

Masoomeh Siminghad, Ashraf S. Shahvelayati*, Shabnam Sheshmani, Roya Ahmadi

Department of Chemistry, Yadegar-e-Imam Khomeini (RAH) Shahre-rey Branch, Islamic Azad University, Tehran, Iran.

ARTICLE INFO

Article History:
Received 2019-05-24
Accepted 2019-07-15
Published 2022-03-01

Keywords:
SnO
Nanosheet
Microflower
1-Pentyl-3 methylimidazolium bromide
Ionic liquid
Photodegradation
Remazol Black B

ABSTRACT

In this study, simple ionic liquid-assisted preparation of SnO microflowers with nanosheet subunits under reflux condition without calcination are described. Samples are synthesized using 1-pentyl-3-methylimidazolium bromide, [pmim]Br, as an ionic liquid in different molar ratios, sodium hydroxide and Tin(II) chloride. The results showed that SnO was obtained with high purity and uniform size distribution using 1:4:4 molar ratios of $SnCl_2$/NaOH/IL by simple reflux method and the ionic liquid only acted as a suitable template. The characterization of the products were carried out by FT-IR, X-ray powder diffraction (XRD), scanning electron microscopy (SEM), energy dispersive X-ray spectroscopy (EDXS) and DRS techniques. Photodegradation of Remazol Black B (RBB) from the aqueous solution was investigated by SnO nanosheets (93.48% dye removal). The rate of degradation of RBB in the presence of SnO is distinctive by the pseudo-first-order kinetic model ($R^2 > 0.79$).

How to cite this article
Siminghad M., Shahvelayati A. S., Sheshmani S., Ahmadi R. Ionic Liquid-assisted Synthesis, Characterization and Photocatalytic Properties of SnO Microflowers with Nanosheet Subunits. J. Nanoanalysis., 2022; 9(1): 1-10.
DOI: 10.22034/jna.2019.1869561.1142.

INTRODUCTION

In the recent decades, much effort has been made toward the synthesis and characterization of nanosized transition metal oxide particles. One of them is Tin(II) oxide (stannous oxide) that contains two forms, a stable black and a meta stable red form. Tin oxide is widely studied, due to its potential applications as gas-sensing material, antistatic film, thin film resisters, anti-reflecting coating in solar cell and p-type semiconductor with wide direct optical band gap of 2.5-3.4 eV [1-4]. Different methods have been reported for the preparation of tin oxide such as *e.g.*, precipitation, sol-gel, sonochemical, microwave, solvothermal, spray pyrolysis, pulsed laser deposition, sputtering and deposition [5-12]. For example, Dai et al. used thermal evaporation to synthesize diskettes-like SnO crystals [13]. Orlandi et al. employed vapor-liquid-solid methods to synthesize belts and dendrites like SnO crystals [14]. Uchiyama et al. used acidic aqueous solution to manipulate the SnO morphology [15]. Nano-square sheets [16] and sheets-like [17] SnO were synthesized by template-free hydrothermal growth method and chemical vapor deposition (CVD), respectively. However, some techniques required complicated experimental methods with high temperature equipment. Also, there are some environmental aspects of the synthesis procedure. It was significant to develop a simple and environmentally method for preparation of nanostructured SnO. One of the new methods that have been recently considered is the use of ionic liquids (ILs) as potential templates. Room temperature ionic liquids (RTILs), especially those based on 1,3-dialkylimidazolium salts, have shown great promise as attractive alternatives to the conventional solvents. Ionic liquids (IL) are receiving increasing interest in nanomaterials synthesis due to their properties such as thermal

* Corresponding Author Email: *avelayati@yahoo.com*

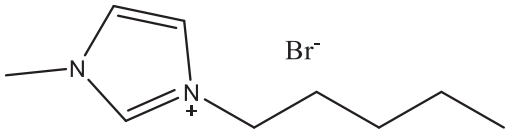

Scheme 1. Structure of 1-pentyl-3-methylimidazolium bromide [pmim]Br.

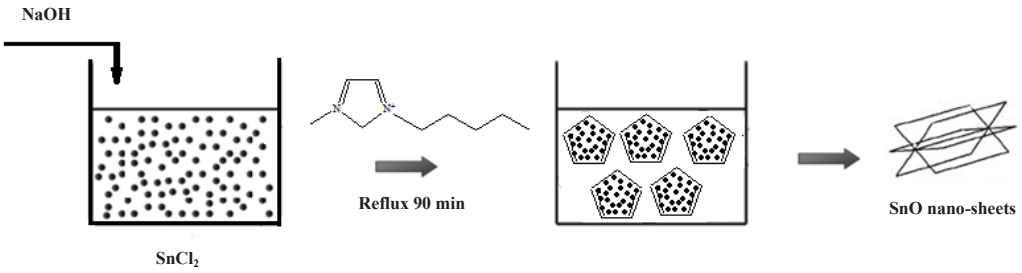

Scheme 2. Illustration for the processes of SnO nanosheets synthesized by IL-assisted growth.

and chemical stability, negligible vapor pressure, immiscibility with both organic and inorganic compounds, non-flammability and recyclability [18, 19]. It is well recognized that the physical properties of a material strongly depends on its size and morphology. ILs have been widely used as templates for the synthesis of nanomaterials. By modifying the structure of the cations or anions of ionic liquids, it has been shown that their properties can be altered in order to influence on morphology, size and optical properties of nanomaterials [20].

Until now, various kinds of metal oxide semiconductor materials such as SnO have been used as a photocatalyst in degradation of dye pollutants [21-25]. However, many researchers have reported that the properties of semiconductors depend on their crystalline structure, size, and morphology, but achieving high photocatalyst activity is still a challenge [26, 27].

As a part of our continuing efforts toward the development of novel, efficient, and green procedure in the rapid ionic liquid assisted synthesis of nanometal oxides [28-30], in this article, nanosheet morphologies of SnO structures have been successfully synthesized by a simple reflux method in water in the presence of 1-pentyl-3-methylimidazolium bromide as an ionic liquid. Different molar ratios of 1-pentyl-3-methylimidazolium bromide and sodium hydroxide were dissolved in water and used as a reaction medium for preparation of SnO nanostructure without calcination.

In recent years, large numbers of photocatalysts, such as ZnO [31], TiO_2 [32, 33], SnO_2 [34], MnO_2, Mn_3O_4 [35] and CuO [36] were investigated in RBB photodegradation. The degradation efficiency was observed above 90% in most cases under irradiation of UV light. In this research, photocatalytic properties of the synthesized SnO under visible light irradiation were investigated in degradation of Remazol Black B (RBB). Some affecting factors such as *p*H, adsorbent dosage, dye concentration and contact time, were studied to optimize the photodegradation conditions. The kinetic of the photocatalytic process of these nanocomposites was also evaluated.

EXPERIMENTAL

Materials

1-Bromopentane ($C_5H_{11}Br$, 99%), 1-methylimidazole ($C_4H_6N_2$, 99%), tetrahydrofuran (C_4H_8O, 99.9%) and diethyl ether) $C_4H_{10}O$ (were purchased from Sigma-Aldrich (Germany). Tin(II) chloride ($SnCl_2$, 99.9%), Sodium hydroxide (NaOH, 97%) and absolute ethanol (C_2H_5OH), were brought from Merck Ltd (Germany). Remazol Black B (RBB) was obtained from Alvand Sabet Company (Iran). All chemicals were commercially available of analytical grade and were used without further purification.

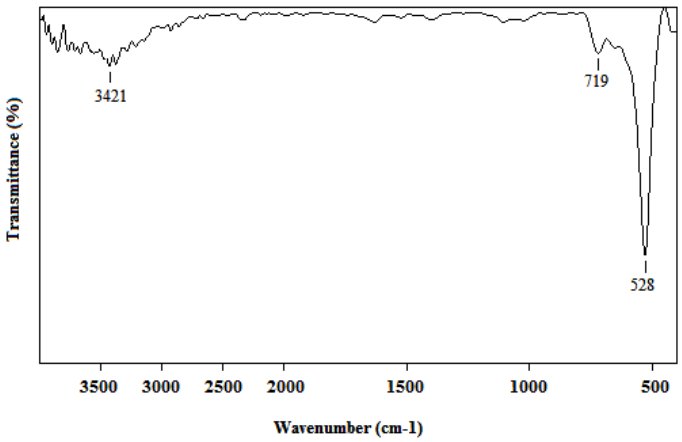

Fig. 1. FT-IR spectrum of SnO.

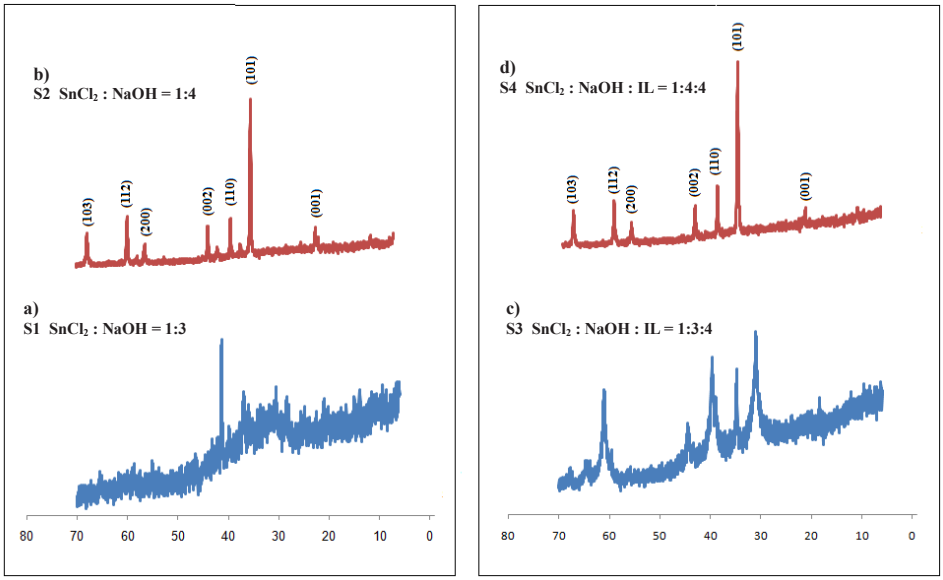

Fig. 2. XRD patterns of S1-S4 samples.

Preparation of 1-pentyl-3-methylimidazolium bromide ionic liquid

The IL used in this study was synthesized according to Menshutkin reaction [37]. A mixture of N-methylimidazole (10 mmol, 0.79 mL) and 1-bromopentane (10 mmol, 1.24 mL) was refluxed for 6 hours in THF under N_2 for the synthesis of 1-pentyl-3-methylimidazolium bromide. The viscose liquid was washed repeatedly with THF (3 × 10 mL). The solvent of the mixture was evaporated under reduced pressure to leave the colorless viscose oil as an ionic liquid. ^{1}H NMR and IR spectroscopic data are used to confirm the structure of ionic liquid (Scheme 1).

1-Pentyl-3-methylimidazolium bromide [pmim]Br:

Viscous oil , Yield: (98%), IR (cm^{-1}) (KBr): 3051, 2929, 2860, 1632, 1490, ^{1}HNMR (500 MHz, $CDCl_3$) δ = 0.88 (3 H, t, ^{3}J = 6.5, CH_3), 1.27-1.32 (6 H, m, $3CH_2$), 3.66 (3 H, s, NCH_3), 3.95 (2 H, t, ^{3}J = 6.5, NCH_2) , 7.24 (2H, s, 2 CH); 9.54 (1H, s, CH) ppm.

Preparation of SnO

A simple approach was used in the preparation of SnO nanosheet by reflux protocol. In this method, $SnCl_2$ was converted to nanosheet by the using of ionic liquid (Scheme 2). The reaction between $SnCl_2$ with sodium hydroxide in the presence and absence of 1-pentyl-3-methylimidazolium

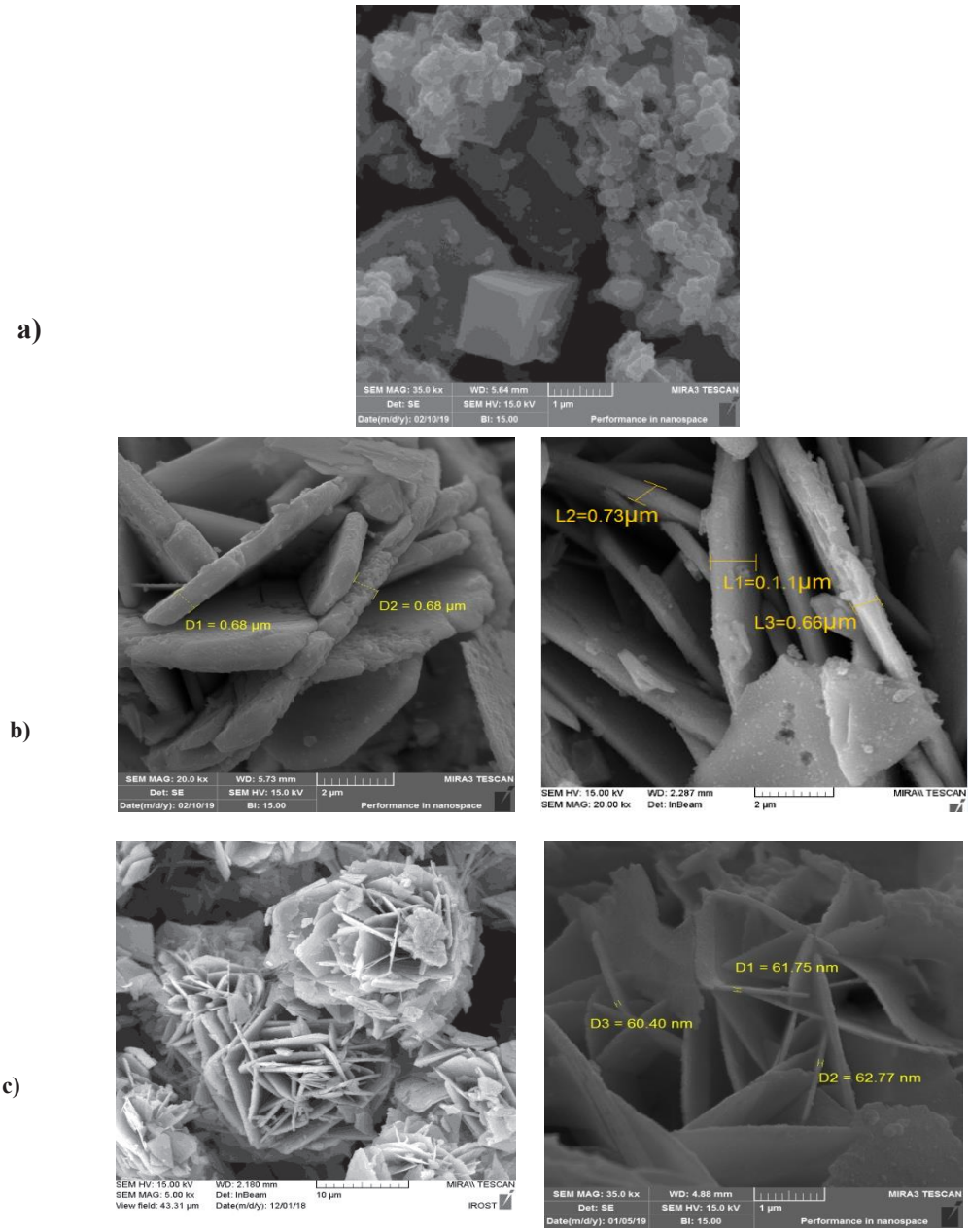

Fig. 3. SEM Micrograph (a) 1:3 molar ratio of $SnCl_2$/NaOH without IL, (b) 1:4:3 molar ratio of $SnCl_2$/NaOH/IL and (c) 1:4:4 molar ratio of $SnCl_2$/NaOH/IL.

bromide at reflux temperature without calcination leads to a preparation of SnO with different size and morphology. The reaction mixture was transferred into a round bottom flask and refluxed for 90 min. After the reaction was complete, the resulting black solid product was washed with distilled water and ethanol. Different molar ratios of $SnCl_2$/NaOH and $SnCl_2$/NaOH/IL as 1:3, 1:4 and 1:3:4 and 1:4:4 were studied in SnO preparation.

Characterizations

Fourier transform-infrared measurements (FT-IR) spectra were recorded (between 500 and 4000 cm^{-1}) on KBr pellets with a Tensor 27 Bruker spectrophotometer. ^{1}H and ^{13}C NMR spectra were recorded with a Bruker DRX-300 Advance instrument using $CDCl_3$ as the deuterated solvent containing tetramethylsilane as internal standard, at 500 MHz, δ in ppm, J in Hz. The crystallographic

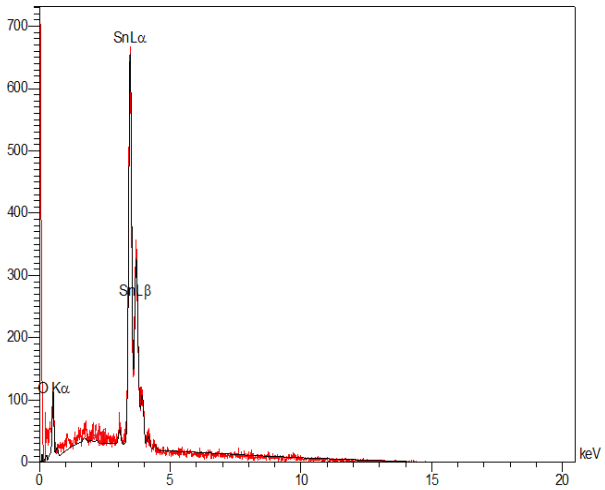

Elt	Line	Int	Error	K	Kr	W%	A%	ZAF	Formula	Ox%	Pk/Bg	Class	LConf
O	Ka	26.7	9.3407	0.0612	0.0480	19.96	64.92	0.2406		0.00	16.39	A	
Sn	La	291.6	1.1643	0.9388	0.7370	80.04	35.08	0.9208		0.00	24.08	A	
				1.0000	0.7851	100.00	100.00			0.00			

Fig. 4. Energy-dispersive X-ray analysis of SnO nanosheet.

structures were observed by X-ray diffraction (XRD, PHILIPS/ PW1800) at room temperature with Cu *Kα* radiation. The morphologies were analyzed by a scanning electron microscope (SEM, TESCAN HV:20.00kV\\MIRA) that was equipped with an energy-dispersive X-ray analysis (EDXS) system. The optical properties of the samples were analyzed by UV/Vis diffuse reflectance spectroscopy (UV-vis DRS) using an Avaspec-2048-TEC spectrophotometer equipped with an integrating sphere attachment. Barium sulfate was used as a reference. The reflectance spectra were converted to equivalent absorption Kubelka-Munk units of the instrument software. The band gap was determined from the plots of transformed Kubelka-Munk as a function of the energy. UV-vis absorption spectroscopy measurements were performed by means of a Varian-Cary Bio 100 UV/V spectrophotometer.

Photocatalytic properties study

The effects of various parameters such as *p*H, adsorbent dosage, dye concentration and contact time on the photodegradation of RBB were investigated. The solution of Remazol Black B (RBB) dye was prepared by dissolving 1 g of dye in 1000 mL of distilled water. All experiments were carried out at room temperature (25 ± 1 °C) using a constant agitation speed of 1000 rpm. Experimental solutions of the desired concentrations were prepared by successive dilutions. All the experiments were carried out in a batch system in order to evaluate the effects of different variables. Tin (II) oxide (5 mg), was dispersed in an aqueous solution of RBB dye (20 ppm, 15 mL) in a conical flask. The reactor content was stirred constantly and then irradiated by mercury lamp at room temperature. The absorbance measurement of the reaction solution was taken after separating the adsorbent from the reaction system by centrifugation. The initial and final RBB concentrations remaining in the solutions were analyzed by a UV spectrophotometer. The photocatalytic activity was evaluated on the basis of the decrease of the absorbance band of the RBB at 597 nm. The adsorption capacity, q_{max}, was calculated from the mass balance at the time (t), given by Eq. (1):

$$q_t = \frac{(C_0 - C_t)V}{W} \qquad \text{Eq. (1)}$$

Where q_t is the amount of dye taken up by the photocatalyst (mg/g), C_0 is the initial dye concentration (mg/L), C_t is the concentration of dye (mg/L) at time t, V is the volume of dye solution (L) in contact with the adsorbent, and W is the mass (g) of the photocatalyst.

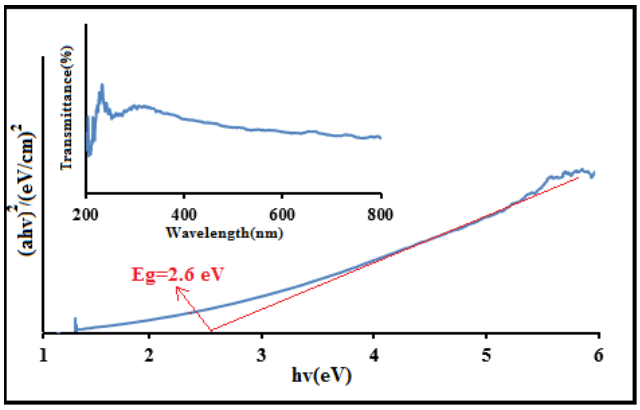

Fig. 5. Plot of transformed Kubelka - Munk as a function of the energy of light and correlation between band gap energy for SnO nanosheet.

RESULTS AND DISCUSSION

IR Spectrum

Fig. 1 shows the FT-IR spectrum of prepared SnO. One peak at 528 cm^{-1} can be observed, which is ascribed to the stretching vibrations of the Sn–O. The absorption band at 3421 cm^{-1} is attributed to O–H stretching vibration of adsorbed water. The presence of ionic liquid molecules in this compound was not confirmed by IR spectroscopy because 1-pentyl-3-methylimidazolium bromide only acted as a template. Therefore, the FT-IR results ensured us of the formation of SnO.

XRD patterns

Fig. 2 shows XRD patterns for S1-S4 samples. The S1 and S2 samples synthesized in the absence of ionic liquid with different molar ratios of $SnCl_2{\cdot}2H_2O$/NaOH in 1:3 and 1:4, respectively. When the molar ratio of $SnCl_2$/NaOH was 1:3, the XRD results confirmed the formation of SnO minor phase as well as $Sn_{21}Cl_{16}(OH)_{14}O_6$, which were not well crystallized, Fig. 2a. When the amount of NaOH in reaction medium increased ($SnCl_2$/NaOH molar ration is 1:4) the crystalline nature of SnO with orientation in (001), (101), (110), (002), (200), (112) and (103) planes at 18.39, 29.86, 33.30, 37.27, 47.91, 50.83 and 57.40° values were observed. Therefore, SnO crystal growth is highly affected by the amount of NaOH in synthesis medium Fig. 2b. On the other hand, S3 and S4 samples were prepared in the presence of ionic liquid. The impurity phase of Cassiterite SnO_2 and minor phase of Romarchite SnO were obvious in the S3 sample, where the reaction was carried out in the 1:3:4 molar ratio of $SnCl_2$/NaOH/IL. The XRD pattern of S4 sample showed the crystals of SnO with a tetragonal Romarchite structure that were prepared in the 1:4:4 molar ratio of $SnCl_2$/NaOH/IL. No characteristic peaks of impurities were detected in the XRD pattern. The XRD pattern of SnO can be indexed to orthorhombic lattice in the space group *Pcam* with the parameters of a = 5.4903Å, b = 5.89200Å, c = 4.75200Å, Z = 4. (JCPDS card file No. 36-1451).

SEM and EDXS Aalysis

The morphology of the prepared SnO structures from the reaction between $SnCl_2$ and sodium hydroxide that was carried by reflux in the absence and presence of ionic liquid, are indicated in Fig. 3. In addition, energy-dispersive X-ray analysis results are shown in Fig. 4.

Fig. 3a shows the obtained structure in the 1:3 molar ratio of $SnCl_2$/NaOH without ionic liquid. It is clear; the product mainly consists of amorphous morphology with small cubic micro-crystals. By increasing sodium hydroxide in reaction media, small amounts of irregular SnO microsheets were obtained with an average of 0.68-1μm diameter (Fig. 3b). Nanosheet-like SnO was obtained when $SnCl_2$/NaOH/IL molar ratio was 1:4:4 (Fig. 3c). SEM micrograph indicated that this compound was consisted of nanosheets with a thickness of 60 nm. Therefore, ionic liquid was influenced by the thickness of the sheets as a template, decreasing from 0.68-1 μm to 60 nm. Therefore, 1-methyl-3-pentylimidazolium bromide acted as a template to yield the decrease in size and regular sheet morphology of SnO crystallites. It is well known that, a convenient way to prepare small sized particles is to add a template, such as ionic liquids. In general, there are two steps in the formation

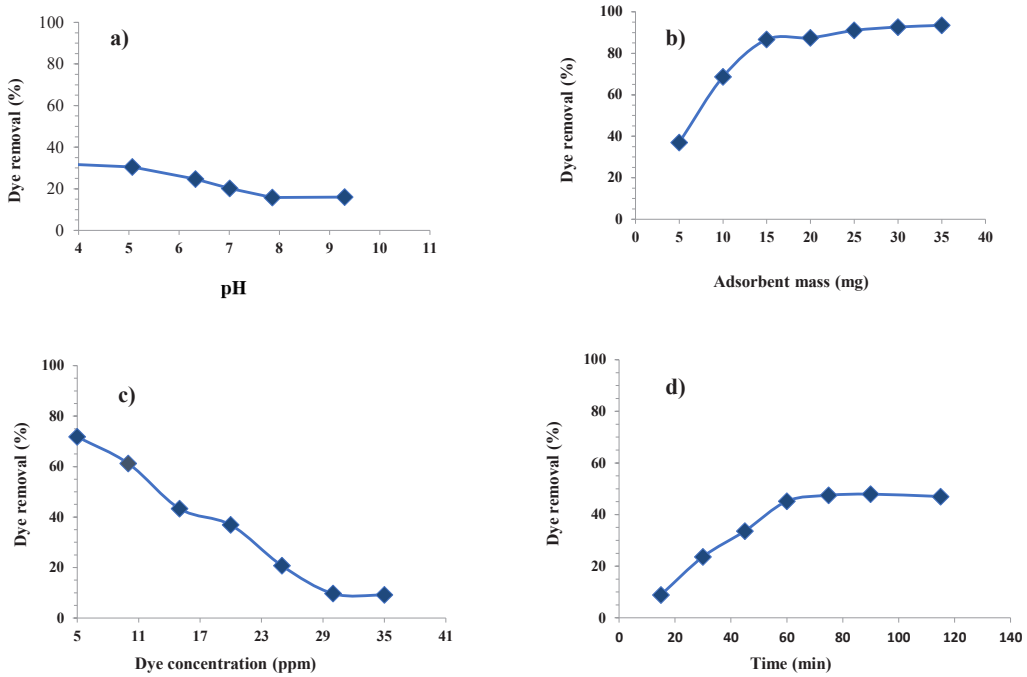

Fig. 6. Effect of (a) *p*H value, (b) adsorbent mass, (c) dye concentration and (d) contact time on RBB removal.

of nanostructures: first, a large crystal nucleus is formed and second, the growth of the formed nucleus. When a template was used in the synthesis procedure, further growth of the crystals was hindered, probably because of the adsorption of the surface-active agent on the surface of the crystal nucleus. The EDX analysis indicated 80.04 W% Sn and 19.96 W% O.

DRS Studies

The band gap energy can be estimated on according to following Eq. (2):

$$\alpha h\nu = B(h\nu\text{-}Ebg)^2 \qquad \text{Eq. (2)}$$

Where $\alpha = (1\text{-}R)^2/2R$, R is the reflectance of the "infinitely thick" layer of the solid [38], *B* is the absorption coefficient, and hν is the photon energy in eV. Fig. 5 plots the relationship of $(ah\nu)^{1/2}$ versus photon energy ($h\nu=1{,}239/\lambda$) [39, 40], which shows that the band gap of SnO is 2.6 eV.

Effect of variable parameters on the photodegradation activity

The effect of various parameters on the photodegradation of RBB in aqueous solution is shown in Fig. 6. The solution *p*H is the key factor in the photocatalytic reaction. To study the effect of *p*H on photodegradation, experiments were carried out in a *p*H range of 3 to 9. Fig. 6(a) showed the relationship between the *p*H value and the dye removal of RBB. Maximum dye removal value was reached at *p*H 5.0 (30.4%). Therefore, in acidic and/or neutral conditions, the interaction between a positively charged photocatalyst surface and negatively charged dye favored adsorption. In an alkaline condition, the adsorption capacity of RBB decreased because the charge of the photocatalyst surface was more negative.

A series of experiments were carried out to find the optimum amount of the photocatalyst by varying the photocatalyst weight between 5 and 35 mg. Fig. 6(b) shows dye removal *vs.* the adsorbent dosage. As can be seen, the dye removal increases as the weight of the photocatalyst increases. Maximum value (93.5%) was obtained at 35 mg of the SnO photocatalyst. With a greater amount of photocatalyst, there was an increase in the active sites.

The effect of the dye concentration is an important parameter in photocatalytic activity. Fig. 6(c) shows the photocatalytic degradation of RBB at different dye concentrations in the range of 5-35 ppm. It is clear that the photodegradation of RBB decreases with increasing concentration of the dye. By increasing the concentration of RBB, more dye

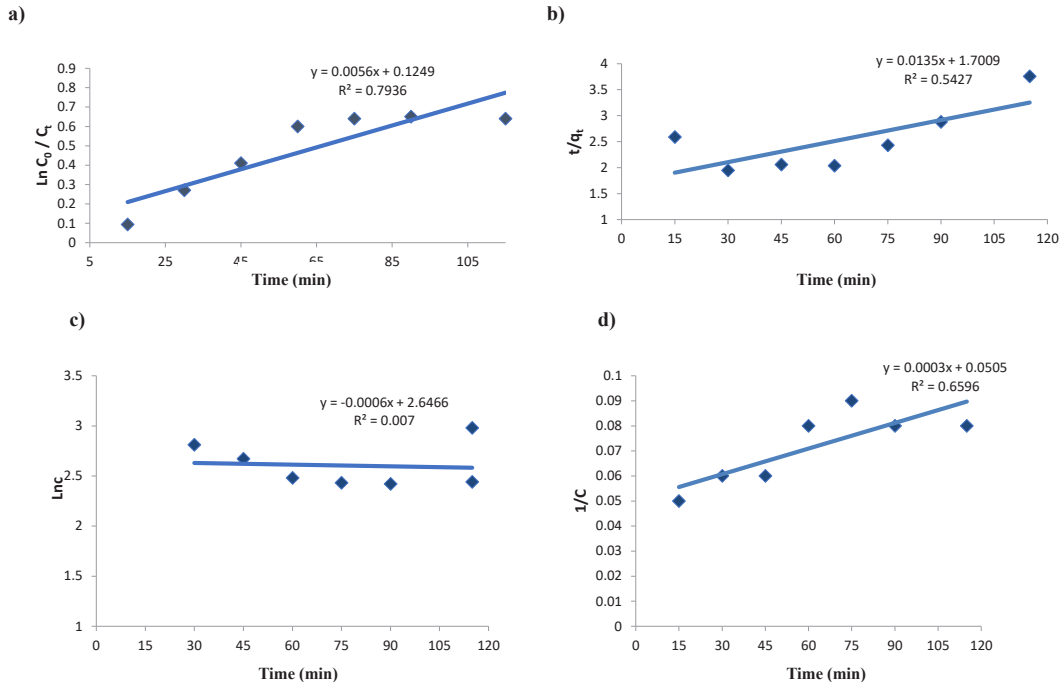

Fig. 7. Kinetic (a) pseudo-first-order, (b) pseudo-second-order, (c) first-order and (d) second-order for RBB degradation using SnO.

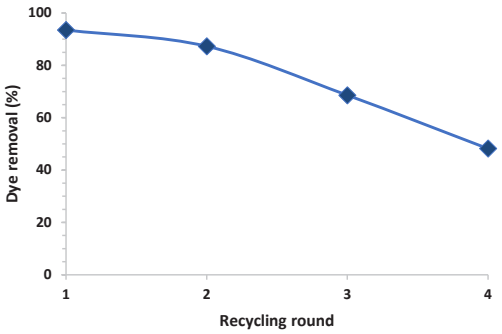

Fig. 8. Recycling round of SnO on RBB photodegradation.

molecules are adsorbed at the photocatalyst surface, resulting in the occupation of the catalyst active sites and consequently decreasing the photocatalyst surface. The effect of contact time (15-120 min) was studied in the photodegradation of RBB. The results reveal that the photodegradation increases with the extension of contact time to 60 min and then remained constant (Fig. 6(d)).

Kinetic studies

The rate of degradation of RBB in the presence of SnO is distinctive by the pseudo-first-order kinetic model as proposed by Eq. (3). Where C_0 is the initial concentration, C_t is the concentration over time (t), and K is rate constant of pseudo-first-order (min^{-1}). The value of K was determined from the slopes of the plot of ln $(C_0 - C_t)$ *vs.* t (Fig. 7).

$$\ln (C_t/C_0) = Kt \qquad \text{Eq. (3)}$$

Regeneration and reuse of SnO

The regeneration and reuse of photocatalysts is quite crucial in practical applications because of ecological and economic demands. It is observed that SnO can be subjected to multiple rounds of reuse (Fig. 8). The photocatalytic capacity decreases for each new cycle. Meanwhile, after four cycles, the photocatalytic capacity reached at 48.2%. These

results show that the photocatalyst can be reused for RBB photodegradation.

CONCLUSIONS

Tin (II) oxide nanosheet has been prepared using a simple reflux in the presence of the ionic liquid. This method produces SnO in good yield with no requirement of high temperature/pressure and calcination. This study demonstrates that the 1-pentyl-3-methylimidazolium bromide may be a suitable template for the formation of SnO with nanosheet morphology. Different molar ratios of ionic liquid and sodium hydroxide in the presence of $SnCl_2 \cdot 2H_2O$ were investigated for preparation of SnO with different size and morphology. The results showed that SnO was obtained with high purity and uniform size distribution using 1:4:4 molar ratios of $SnCl_2$/NaOH/IL by simple reflux method. X-ray diffraction (XRD) analysis confirmed the crystalline nature of SnO with orientation in (001), (101), (110), (002), (200), (112) and (103) planes at 18.39, 29.86, 33.30, 37.27, 47.91, 50.83 and 57.40° values. Microflowers were elucidated with nanosheet subunits (thickness of sheets ~60 nm) by scanning electron microscope (SEM). The products may be good candidates for photocatalytic applications in dye removal.

CONFLICT OF INTEREST

The authors declare that there is no conflict of interests regarding the publication of this manuscript.

REFERENCES

1. L.Y. Liang, Z.M. Liu, H.T. Cao, Y.Y. Shi, X.L. Sun, Z. Yu, A.H. Chen, H.Z. Zhang and Y.Q. Fang, ACS Appl. Mater. Interfaces, 2, 1565 (2010). https://doi.org/10.1021/am100236s
2. S.H. Park, Y.C. Son, W.S. Willis, S.L. Suib and K.E. Creasy, Chem. Mater., 10, 2389 (1998). https://doi.org/10.1021/cm970672x
3. S. Seal and S. Shukla, JOM., 54, 35 (2002). https://doi.org/10.1007/BF02709091
4. A. Shanmugasundaram, P. Basak, L. Satyanarayana and S.V. Manorama, Sens. Actuators B., 185, 265 (2013). https://doi.org/10.1016/j.snb.2013.04.097
5. K. Nejati, Cryst. Res. Technol., 47(5), 567 (2012). https://doi.org/10.1002/crat.201100633
6. M. Aziz, S. Saber Abbas, W. Rosemaria and W. Baharom, Mater. Lett., 91, 31 (2013). https://doi.org/10.1016/j.matlet.2012.09.079
7. S. Majumdar, S. Chakraborty, P.S. Devi and A. Sen, Mater. Lett., 62 (8-9), 1249 (2008). https://doi.org/10.1016/j.matlet.2007.08.022
8. D. Han, Y. Wang, C. Sun, B. Liang and W. Zhang, Ceram. Int., 45(3), 4089 (2019). https://doi.org/10.1016/j.ceramint.2018.10.204
9. S-Z. Kang, Y. Yang and J. Mu, Colloids and Surf. A: Physicochemical and Engineering Aspects, 298(3), 280 (2007). https://doi.org/10.1016/j.colsurfa.2006.11.008
10. S.P. Choudhury, S.D. Gunjal, N. Kumari, K.D. Diwate, K.C. Mohite and A. Bhattacharjee, Mater. Today Proceeding 3(6), 1609 (2016). https://doi.org/10.1016/j.matpr.2016.04.050
11. M.A. El Khakani, R. Dolbec, A.M. Serventi, M.C. Horrillo, M. Trudeau, R.G. Saint-Jacques, D.G. Rickerby and I. Sayago, Sensors and Actuators B Chemical, 77(1), 383 (2001). https://doi.org/10.1016/S0925-4005(01)00758-4
12. D. Leng, L. Wu, H. Jiang, Y. Zhao, J. Zhang, W. Li and L. Feng, Int. J. Photoenergy doi: 10.1155/2012/235971 (2012). https://doi.org/10.1155/2012/235971
13. Z.R. Dai, Z.W. Pan and Z.L. Wang, J. Am. Chem. Soc., 124, 8673 (2002). https://doi.org/10.1021/ja026262d
14. M.O. Orlandi, E.R. Leite, R. Aguiar, J. Bettini and E. Longo, J. Phys. Chem. B, 110, 6621 (2006). https://doi.org/10.1021/jp057099m
15. H. Uchiyama, H. Ohgi and H. Imai, Cryst. Growth. Des., 6, 2186 (2006). https://doi.org/10.1021/cg060328p
16. M.Z. Iqbal, F.P. Wang, T. Feng, H.L. Zhao, M.Y. Rafique, R.U. Din, M.H. Farooq, Q.U. Javed and D.F. Khan, Mater. Res. Bull., 47, 3902 (2012). https://doi.org/10.1016/j.materresbull.2012.07.002
17. B. Kumar, D.H. Lee, S.H. Kim, B. Yang, S. Maeng and S.W. Kim, J. Phys. Chem. C, 114, 11050 (2010). https://doi.org/10.1021/jp101682v
18. P. Wasserscheid and T. Welton, Wiley, Weinheim (2003).
19. J. Dupont, R.F. de Souza and P.A.Z. Suarez, Chem. Rev., 102, 3667 (2002). https://doi.org/10.1021/cr010338r
20. Q. Li, V. Kumar, Y. Li, H. Zhang, T.J. Marks and R.P.H. Chang, Chem. Mater., 17, 1001 (2005). https://doi.org/10.1021/cm048144q
21. S. Sheshmani and M. Nayebi, Polym. Composites, 210 (2019).
22. S.K. Kansal, M. Singh and D. Sud, J. Hazard. Mater., 141(3), 581 (2007). https://doi.org/10.1016/j.jhazmat.2006.07.035
23. S.M. Hassan and M.A. Mannaa, Int. J. Nano and Mater. Sci., 5(1), 9 (2016).
24. N. Assi, P. Aberoomand Azar, M. Saber Tehrani, S.W. Husain, M. Darwish and S. Pourmand, Int. J. Nano Dimens., 8(3), 241 (2017).
25. A. Radhakrishnan, P. Rejani and B. Beena, Int. J. Nano Dimens., 9(2), 145 (2018).
26. S. Majumdar, Ceram. Int., 41, 14350 (2015). https://doi.org/10.1016/j.ceramint.2015.07.068
27. B. Munirathinam, H. Pydimukkala, N. Ramaswamy and L. Neelakantan, Appl. Surf. Sci., 355, 1245 (2015). https://doi.org/10.1016/j.apsusc.2015.08.017
28. M. Sabbaghan, A.S. Shahvelayati and S. Banihashem, Ceram. Int., 42, 3820 (2016). https://doi.org/10.1016/j.ceramint.2015.11.046
29. M. Sabbaghan, A.S. Shahvelayati and K. Madankar K., Spectrochimica Acta Part A: Molecular and Biomolecular Spectrosc., 135, 662 (2015). https://doi.org/10.1016/j.saa.2014.07.097
30. M. Sabbaghan, A.S. Shahvelayati and S.E.

Bashtani, Solid State Sci., 14, 1191 (2012). https://doi.org/10.1016/j.solidstatesciences.2012.05.034
31. M. Obaidullah, M.J. Miah, M.N. Kayes, N. Suzuki and M.M. Hossain, J. Adv. Chem. Sci., 3(1), 445 (2017).
32. M.J. Miah, M.T. Aziz, M.N. Kayes, M. Obaidullah and M.M. Hossain, British J. Environ. Sci., 5(2), 51 (2017).
33. S.K. Kansal, N. Kaur and S. Singh, Nanoscale Res. Lett., 4(7), 709 (2009). https://doi.org/10.1007/s11671-009-9300-3
34. S.R. Khan, M.U. Khalid, S. Jamil, S. Li, A. Mujahid and M.R.S. Ashraf Janjua, J. Water and Health, 16, 773 (2018). https://doi.org/10.2166/wh.2018.033
35. H. Saroyan, D. Ntagiou, K. Rekos and E. Deliyanni, Appl. Sci., 9(10), 2167 (2019). https://doi.org/10.3390/app9102167
36. M.P.C. Rao, K. Kulandaivelu, V.K. Ponnusamy, J.J. Wu, A. Sambandam, Environ. Sci. Pollut. Res. Doi:10.1007/s11356-019-05434-1 (2019). https://doi.org/10.1007/s11356-019-05434-1
37. Y.S. Vygodskii, E.I. Lozinskaya and A.S. Shaplov, Macromol. Rapid. Commun., 676 (2002). https://doi.org/10.1002/1521-3927(20020801)23:12<676::AID-MARC676>3.0.CO;2-2
38. A. A. Christy, O.M. Kvalheim and R.A. Velapoldi, Vib. Spectrosc., 9, 19 (1995). https://doi.org/10.1016/0924-2031(94)00065-O
39. K.M. Reddy, S.V. Manorama and A.R. Reddy, (2003), Mater. Chem. Phys., 78, 239 (2003). https://doi.org/10.1016/S0254-0584(02)00343-7
40. J. Tauc, R. Grigorov and A. Vancu, Phys. Status. Solidi, 15, 627 (1966). https://doi.org/10.1002/pssb.19660150224